



The Effects Welding Speed and Focal Length on Mechanical Characteristic of Fiber Laser-Welded Structures of DP600 Dual Phase Steel

Elif Selen ATMACA^{1*} , Adem KURT² 

¹Gazi University, Graduate School of Natural and Applied Sciences, Ankara, Turkey

²Gazi University, Faculty of Technology, Department of Metallurgical and Materials Engineering, Ankara, Turkey

Keywords	Abstract
DP600 DP Steels Fiber Laser Welding Welding Speed Focal Length	In this study, the effect of welding speed (3, 3.5, 4 m/min) and focal length (0, 1.4 mm) on the mechanical properties of the welded structure was investigated in the overlap type joining of 1.2 mm sheet thickness DP600 dual phase steel sheet material by fiber laser welding method. For this purpose, tensile-shear tests were performed on the samples joined by laser welding method, and the tensile strength and elongation amounts were determined. Microstructure investigation and microhardness measurements of the welded area were carried out. It is determined that weld joint shape and penetration depth changes according to focal length distance and welding speed, and with the maximum welding speed specimens has the minimum penetration depth. Tensile-shear strength values decreased depending on the increased welding speed for both focal length specimens. It is observed that the microhardness results were affected by welding speed and focal lengths. In 0 mm focal length distance specimens' hardness values increased according to the increased welding speed, but for -1.4 mm focal length distance the microhardness values decreased with an increased welding speed. The fracture zones and fracture surface morphology also affected by welding speed and focal distance. In 0 mm focal length, all the specimen fractured in base metal with a ductile fracture morphology, but in the -1.4 mm focal length, specimens fractured from the zones which are closer to HAZ and FZ with a brittle fracture morphology.

Cite

Atmaca, E. S., & Kurt, A. (2021). The Effects Welding Speed and Focal Length on Mechanical Characteristic of Fiber Laser-Welded Structures of DP600 Dual Phase Steel. *GU J Sci, Part A, 8(1)*, 146-156.

Author ID (ORCID Number)

E. S. Atmaca, 0000-0002-1892-9091
 A. Kurt, 0000-0002-1439-4683

Article Process

Submission Date 30.12.2020
Revision Date 14.03.2021
Accepted Date 25.03.2021
Published Date 29.03.2021

1. INTRODUCTION

The one of the purposes of the new generation materials used in the automotive industry is to reduce the fuel consumption and carbon emissions associated with it by reducing the vehicle weight. Therefore, the use of new generation materials that provide high strength in thinner sections is rapidly increasing (Gong et al., 2016).

Today, dual phase steels have an important place among the high strength steels and they are provided with superior mechanical properties such as high strength / weight ratio, low yield / ultimate strength ratio. These steels are produced with a sufficient cooling rate to convert the austenite to martensite phase after the ferrite + austenite structure is annealed between Ac_1 and Ac_3 temperatures. Thus, the martensite phase created in the material provides strength to the steel, while the soft ferrite matrix provides ductility (Fonstein, 2017; Çavuşoğlu et al., 2019; Dai et al., 2020).

Although different welding methods such as resistance spot welding, gas metal arc welding and friction stir welding are used for joining metallic materials, laser welding method is also preferred by automotive manufacturers considering the production speed and welding performance (Hong & Shin, 2017; Kancharla et al., 2018; Aktarer et al., 2019; Kuril et al., 2019; Zhao et al., 2019).

The studies on joining of steel sheets by laser welding method in the literature are abundant. Mitra et al. (2020a) determined that with increasing laser welding speed, the surface defects increased in the HAZ region and this situation facilitated the fracture in this region. Mitra et al. (2020b) showed in their study, which examines the relationship between welding speed and residual stress, concluded that a lower residual stresses occur at high welding speeds. Tuncel & Aydin (2020) investigated the laser weldability of DP600 double-phase steels in one sided and double sided forms and determined that as the pulse frequency of the laser beam increased, the tensile strength values increased depending on the increase in the area of weld zone. Alves et al. (2018) have optimized laser power and welding speed to minimize prior martensite softening and HAZ (Heat Affected Zone) in the laser weldability of DP1000 dual-phase steel. In the study of Wang et al. (2016), it was observed that DP1000 dual phase steel was subjected to coarse grain structure in laser welding with the increase of energy input and its mechanical properties were weakened. Zhao et al. (2013) determined that in the laser welding process of dual phase steels, the width of FZ (Fusion Zone) is decreased with the increase in welding speed, tensile-shear load decreases and maximum hardness values were obtained at FZ. According to Švec et al. (2015), due to the increase in welding speed, the amount of spatter around the weld seam increased, the weld pool width decreased, cap concavity and root sagging occurred, however, the highest hardness values were determined in FZ and the main material tensile strength was higher than the welded material. In the study by Xie et al. (2017) (3, 4, 5 m/min), no significant effect of laser welding speed on DP590 dual phase steel tensile strength was observed.

The studies in the literature showed that, laser power, pulse frequency, focus length and welding speed affect the mechanical properties of laser welded joining (Zhao et al., 2013; Švec et al., 2015; Wang et al., 2016; Fonstein, 2017; Hong & Shin, 2017; Xie et al., 2017; Alves et al., 2018; Kancharla et al., 2018; Aktarer et al., 2019; Çavuşoğlu et al., 2019; Kuril et al., 2019; Zhao et al., 2019; Dai et al., 2020; Mitra et al., 2020a; Tuncel & Aydin, 2020).

In this study, the effect of different welding speeds (3, 3.5, 4 m/min) and focal lengths (0 - 1.4 mm) on the mechanical and microstructural properties of DP600 dual phase steel sheet combined with fiber laser welding was examined in detail.

2. MATERIALS AND METHODS

2.1. Material

In this study, DP600 dual phase steel with a thickness of 1.2 mm was used. The full chemical composition was determined by spectral analysis. The chemical composition of DP600 is shown in Table 1. The coating mass determined according to ASTM E1659-12 (2012), and the Zn coating of DP600 was measured as 51 g/m²; Zn coating is present on the surface of DP600. Grinding and polishing processes were conducted for the metallographic imaging process of the base DP600 dual phase steel. Etching process was conducted with 2 % Nital solution for 3 sn. The light colored areas represent the ferrite and darker areas the martensite phases on the optical microstructural images of dual-phase steel in as received form given in Figure 1. Ultimate tensile strength determined according to ASTM E8 (2010) standard, and the average ultimate tensile strength was calculated as 691.31 MPa.

Table 1. Chemical Composition of DP600 Dual-Phase Steel (wt, %)

Steel	C	Mn	N	Cr	Si	Mo	Al
DP600	0.069	1.845	0.55	0.217	0.241	0.013	0.03

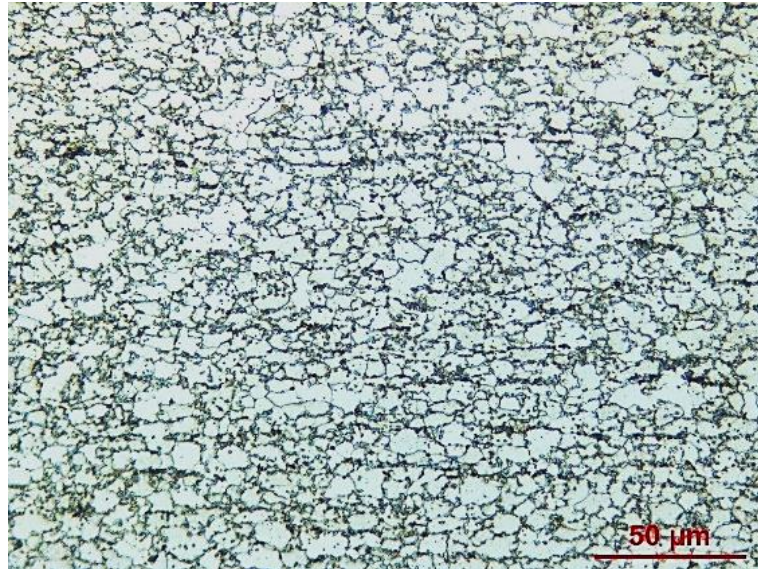


Figure 1. Optical Microstructure Image of DP600 Steel (as received)

2.2. Welding Procedure

Fiber laser welding operations carried out using IPG Photonics YLS 400 laser welding source. The fiber lasers with an emission wavelength of 1070 nm can deliver continuous wave mode through an output fiber core diameter of 100 μm . The focal diameter of the laser beam was 640 μm . The focus position during the welding was kept on the surface and -1.4 mm under the surface of samples. The fiber laser welding machine is shown in Figure 2.

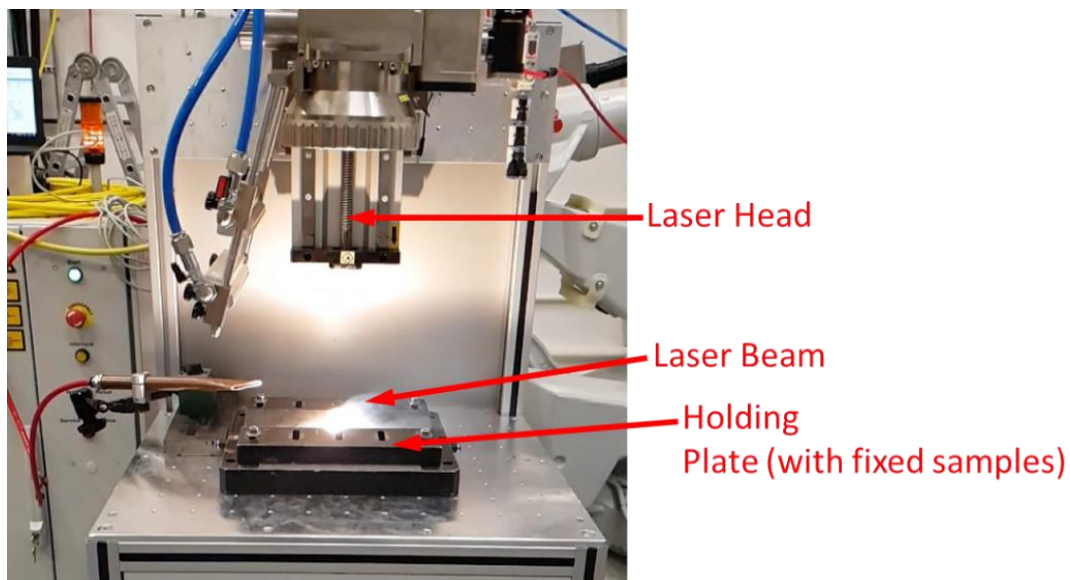


Figure 2. IPG Photonics YLS 400 Fiber Laser Welding Machine

To perform fiber laser welding processes, sheet plates were prepared on the rolling direction in the dimension 221 x 105 mm and steel-on-steel overlap joint of two samples with the overlap length of 35 mm. Schematic representation of the placement of the sheets to the fiber welding laser device is given in Figure 3. Before welding, the surface of all samples were cleaned with acetone to remove grease and residues. The joints were produced by keyhole welding method without filler metal and shielding gas. 0.2 mm shim plates were located between two sheets. Welding parameters and specimen codes were given in Table 2. Laser beam geometry regarding to focal length is also shown in Figure 4. As it stated in Figure 4, when the focal length sets as 0 mm, laser beam focus on the top of the upper sheet; but when the focal length sets as -1.4 mm, laser beam focus on the top of the lower sheet.

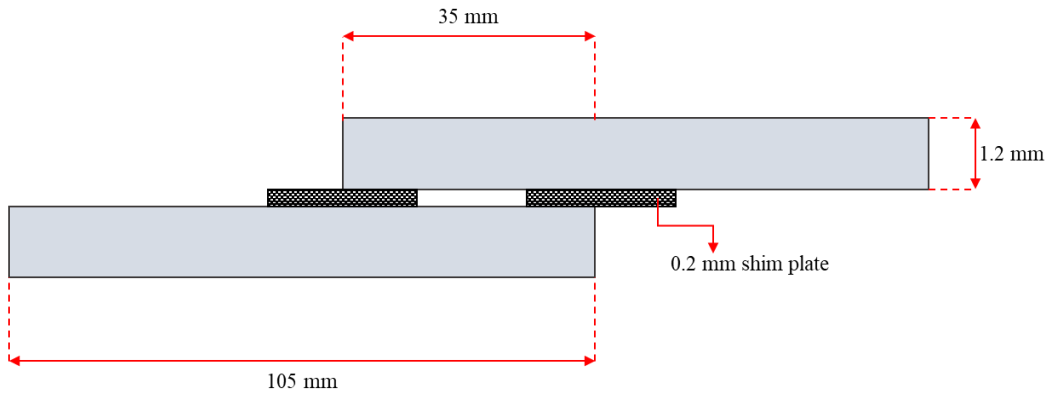


Figure 3. Placement of Sheets into the Fiber Laser Welding Machine

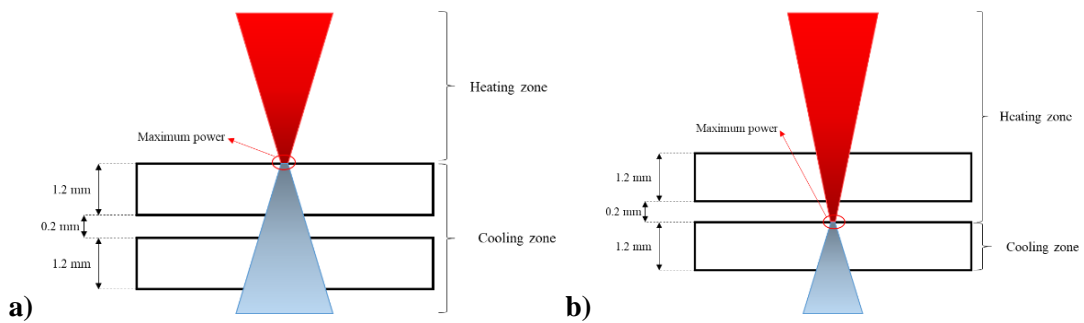


Figure 4. Laser Beam Geometry Differences According to Focal Length,
a) Focal Length: 0 mm, b) Focal Length: -1.4 mm

Table 2. Welding Parameters and Specimen Codes

Laser Power (kW)	Focal Length (mm)	Wave Length (nm)	Spot Size (μm)	Welding Speed (m/min)	Specimen Codes
4	0	1070	640	3	D1
				3.5	D2
				4	D3
4	-1.4	1070	640	3	D4
				3.5	D5
				4	D6

From the welded samples, the tensile-shear test samples were machined with water jet cutting method in the size of 30 x 175 mm according to EN ISO 14273 (ISO, 2016). The tests were performed on the INSTRON 3369 universal testing machine. All tensile-shear tests were carried out perpendicular to the welding direction. The strain rate was chosen as 0.0067s^{-1} according to EN ISO 6892-1 (ISO, 2019). In order to minimize error margin, three tests were performed for each parameter and average results were considered.

The Vickers hardness measurement across the weld zone and base metal were carried out on polished and etched samples using 4.903 N ($\text{HV}_{0.5}$) with a 10 second dwelling time. Average micro hardness value of base metal is measured as $210 \text{HV}_{0.5}$.

The microstructural investigation of welding was performed on the Leica optical microscope and the fracture surface investigation of the tensile-shear tested samples were carried out on the JEOL JEM 6060 scanning electron microscope.

3. RESULTS AND DISCUSSION

3.1. Mechanical Properties

Tensile-shear tests were performed to determine the effect of welding speed and focal length parameters on DP600 dual phase steel sheets. Maximum tensile-shear load – crosshead displacement results for both focal length and different welding speed parameters are shown in Figure 5.

When the Figure 5 is examined, it is seen that there is a decrease in the crosshead displacement values due to the increase in welding speed, and tensile-shear load values were determined as 24.52 kN, 23.82 kN and 23.66 kN for D1, D2 and D3 (Figure 5a), respectively. While for D4, D5 and D6, tensile-shear load values were determined as 246.37 kN, 24.39 kN and 24.15 kN (Figure 5b), respectively. The difference of tensile-shear load between D1 and D3 is almost 4 %, meanwhile 2 % for D4 and D6. The crosshead displacement values showed a similar tendency to the tensile-shear load values. Crosshead displacement values were measured for D1, D2, D3 as 28.63 mm, 26.91 mm and 16.23 mm (Figure 5a), respectively. Crosshead displacement values were also measured for D4, D5, D6 as 29.20 mm, 20.02 mm and 18.44 mm (Figure 5b), respectively. As the welding speed at 0 mm focal length increases, the crosshead displacement decreases approximately 43.5 %, while this ratio is calculated to be 36.83 % at -1.4 mm focal length.

Lakshminarayana et al. (2018) also determined that with the increase in the welding speed caused the incomplete penetration. For this reason, incomplete penetration occurs due to the increase in the welding speed at both focal lengths (Table 3) and thus a decrease in the maximum tensile-shear load and crosshead displacement values occurs.

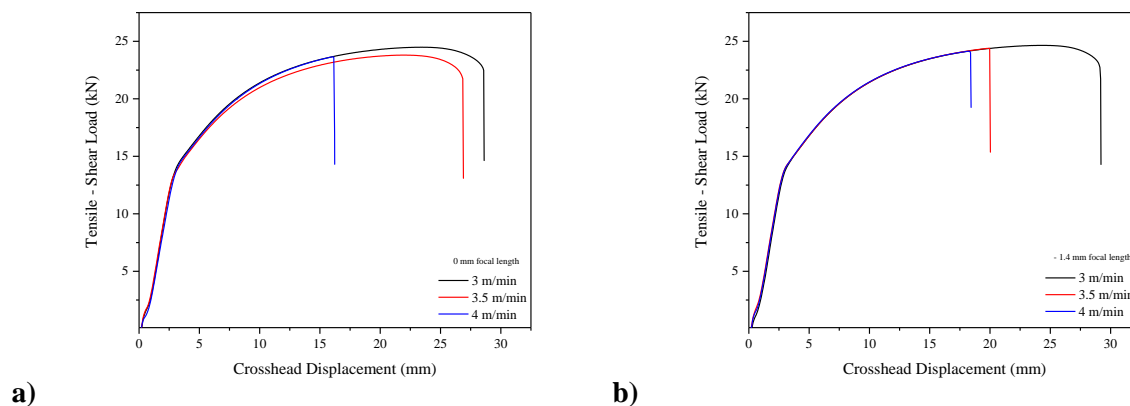


Figure 5. Tensile-Shear Load - Crosshead Displacement curves,
a) Focal Length: 0 mm, b) Focal Length: -1.4 mm

In Figure 6, lap joint fiber laser welded DP600 macrostructure and weld zones have been showed. Base material zones were not affected by heat input and cooling rates and the microstructure is the same as-received material. HAZ were partially affected by heat input and cooling rates. Because of this, the phase transformations and grain size differences can be detected clearly. Since the highest heat input and the highest cooling rate occur in FZ, the fundamental changes can be seen in this region.

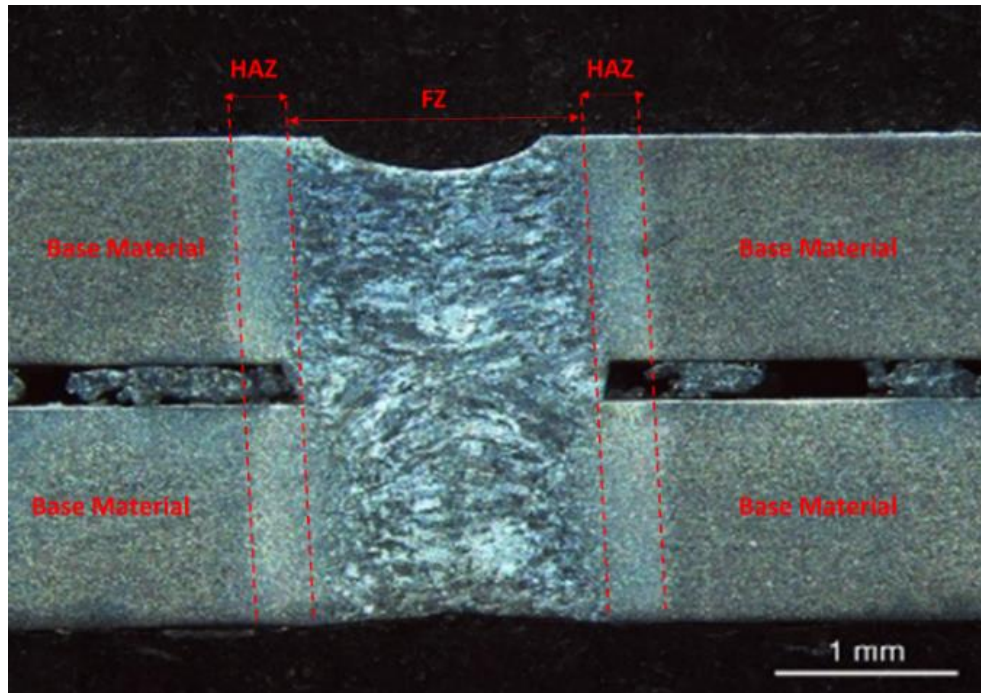


Figure 6. Zone of Welding Structure: Base Material (BM), Heat Affected Zone (HAZ), Fusion zone (FZ)

In Figure 7, microhardness values are shown depending on the welding speed and focal distance conditions. When Figure 7 is examined, a higher hardness value in weld zone (FZ) was observed than HAZ and base material, due to the fact that the cooling rate in the FZ region is the highest at both focal distances. The base metal hardness values, which were not exposed to any thermal effects, have the lowest hardness values. During the welding process, due to the heat input and cooling rate, regions such as HAZ or FZ formed where phase transformations occur.

For 0 mm focal length, FZ and HAZ hardness values measured. According to measurement results, hardness values of HAZ for D1 sample are 316 and 325 HV_{0.5}, and FZ hardness value is 329 HV_{0.5}; hardness values of HAZ for D2 sample are 322 and 338 HV_{0.5}, and FZ hardness value is 347 HV_{0.5}; hardness values of HAZ for D3 sample are 339 and 350 HV_{0.5}, and FZ hardness value is 355 HV_{0.5}.

During the optical analysis, the base metal consists of ferrite matrix and embedded martensite phases (Figure 1). Also Farabi et al. (2011), Gong et al. (2016) and Ferreira et al. (2020) determined fully lath martensitic structure in FZ, and ferrite, lath martensite, tempered bainite in HAZ and according to Sun et al. (2016) during these phase transformations, it is thought that the hardness value increases due to the decrease in the ferrite amount in the HAZ due to the heat input and cooling rates, but the hardness values are lower than FZ due to the tempered phases occurring in this region.

As seen in Figure 7, for -1.4 mm focal length specimens, the micro hardness values decrease as the welding speed increased. Hardness values of HAZ for D4 sample are 381 and 386 HV_{0.5}, and FZ hardness value is 422 HV_{0.5}; hardness values of HAZ for D5 sample are 367 and 363 HV_{0.5}, and FZ hardness value is 400 HV_{0.5}; hardness values of HAZ for D6 sample are 330 and 337 HV_{0.5}, and FZ hardness value is 367 HV_{0.5}.

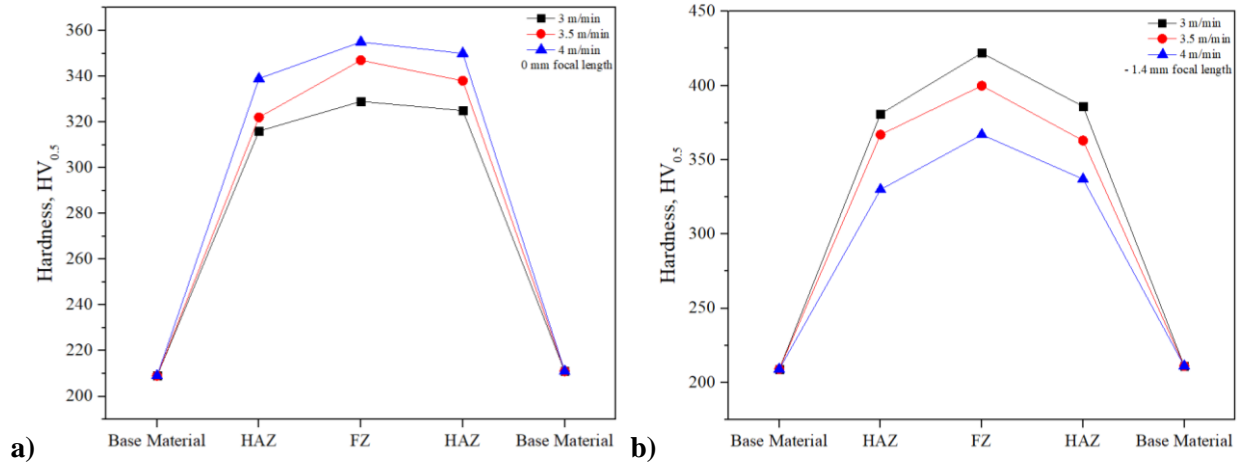


Figure 7. Hardness Distribution on Welded Structure,
a) Focal Length: 0 mm, b) Focal Length: -1.4 mm

It was calculated that the cooling rates increased due to the increase in the welding speed, but the values at this negative focal distance decreased by approximately 21.3 % in all welding speeds compared to the cooling rates of 0 mm focal length samples. Considering the weld regions, the base material consists of ferrite and martensite, and the average hardness values obtained in these regions were considered the same in both focal length samples. When the HAZ and FZ were examined, it was observed that the hardness values decreased due to the increase in the welding speed. When the weld pool where the most prominent transformation (ferrite to lath martensite transformations) occurs in all samples are examined, it is thought that carbide formation occurs besides lath martensite (Figure 8). Although there is an increase in the cooling rate, it is thought that this cooling rate is not enough to keep the structure completely in the martensite phase, the dissolution starts to form carbide and therefore a decrease in hardness values occurs. A similar situation has been observed in HAZ. Tempered martensite phase was observed in the fine-grained region forming the HAZ, different from the sample realized by using 0 mm focal length (Sun et al., 2016; Kundu et al., 2019). For this reason, the hardness values obtained in this region are lower than those of the 0 mm focal distance sample and it is thought that due to the relative decrease in the cooling rate, the tempered martensite phase formed in this region causes a decrease in the hardness values as the welding speed increases, due to the formation of a higher amount. The similar results were also determined in some experimental studies (Kundu et al., 2019; Ferreira et al., 2020; Palanivel et al., 2020).

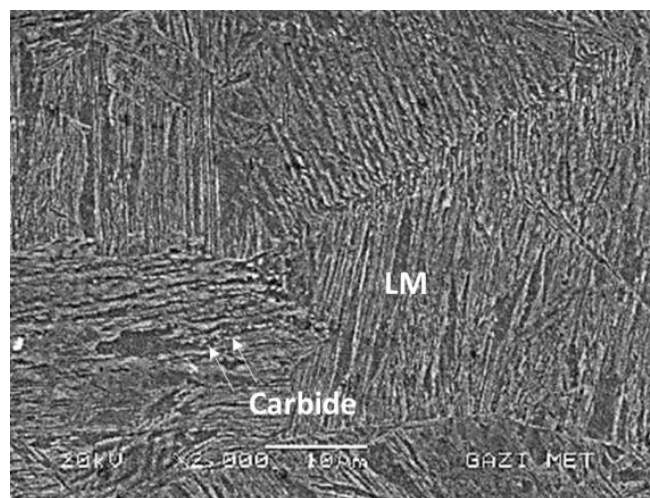
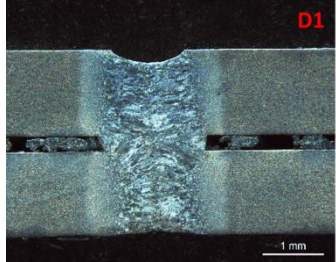
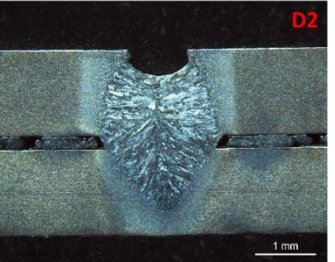
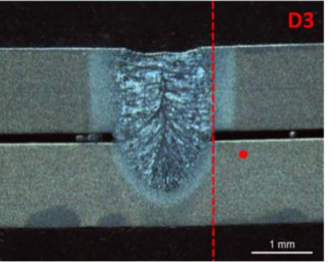
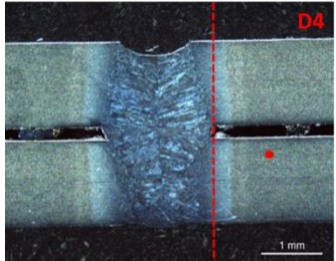
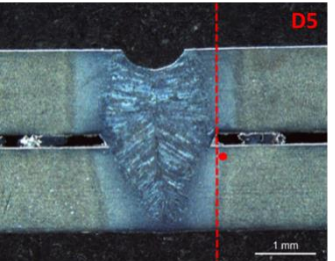
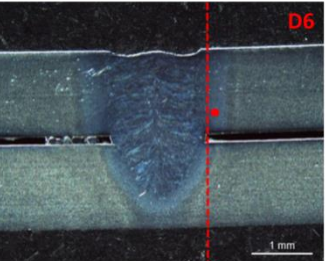


Figure 8. SEM Image of Lath Martensite (LM) and Carbide in FZ

Optical macro structure images depending on welding speed and focal distance parameters and fracture zones of the samples after the tensile-shear tests are shown in Table 3, and reference lines to measure the distances to fracture zone is indicated as red line and fracturing points of samples are marked with red dots.

Fusion zones of D1 and D4 are almost hourglass shaped (Palanivel et al., 2020) and it is seen that the penetration depth in the bottom sheet decreases due to the increase in the welding speed at both focal lengths. Although shrinkage cavity is also observed in D1 and D4, this indication is observed to have the highest depth in D2 and D5 samples.

Table 3. Macro Images and Fracture Zones of Samples

		Welding Speed		
		3 m/min	3.5 m/min	4 m/min
Focal length	0 mm			
	-1.4 mm			

In Figure 9, the distances of the fracture zones of the samples to the Heat Affected Zone (HAZ) are given. Although the fracture approached towards the weld pool as the welding speed increased in the samples with 0 mm focal length, it was still observed that it broke off from the base material. D1, D2 and D3 Fracture Zone-HAZ distances at 0 mm focal length are 30710 μm , 18220 μm and 341 μm , respectively. In D3 sample, it is seen that the fracture is very close to HAZ. When the SEM images were examined, ductile fracture morphology was observed for D1 and D2 (Figure 10a and Figure 10b). Therefore, as expected, fractures in the base material have ductile fracture morphology and similar dimple sizes (Wang et al., 2017). As supported by tensile-shear load – crosshead displacement data, the lowest tensile-shear load – crosshead displacement value is in the D3 sample. The main reason for this situation is that the depth of penetration in the lower sheet is in this sample as seen in Table 3. Because of lack of penetration, the fracture zone got closer to the HAZ and so the D3 fracture surface has brittle fracture morphology (Figure 10c).

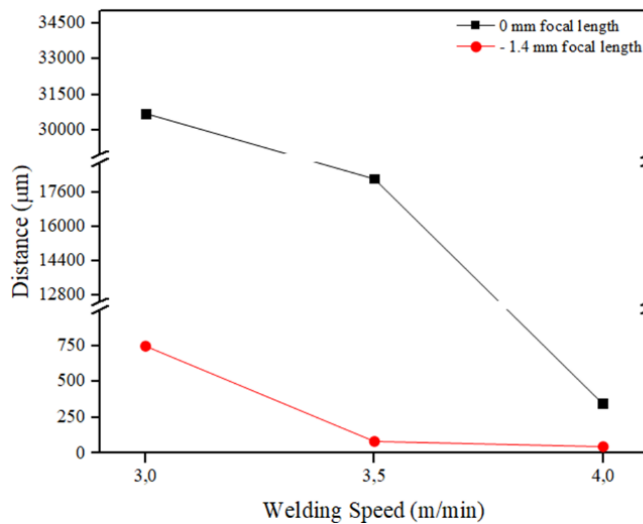


Figure 9. Fracture Distance to Heat-Affected Zone (HAZ)

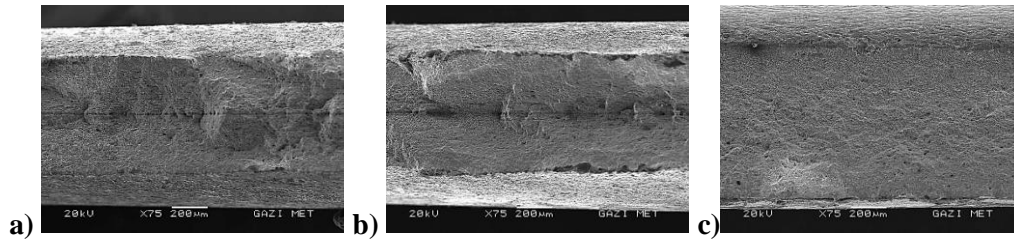


Figure 10. Fracture Surface of 0 mm Focal Length Specimens After Tensile - Shear Load Test, a) D1 Sample, b) D2 Sample, c) D3 Sample

In the samples produced with – 1.4 mm focal length, D4 is fractured from the base material, D5 from the partially transformed region and D6 from the coarse grained region. Also fracture zone and fusion zone distances were measured as 745 μm , 82 μm , and 45 μm respectively. When the SEM images are examined (Figure 11), D4 was fractured from the base material with a ductile morphology (Figure 11a), and this result can be supported with tensile-shear load – crosshead displacement values. The rupture region of the D5 sample is considered to be the partially transformed region. As a result of the SEM analysis, it is thought that the ferrite, martensite and temper martensite phases that are likely to occur in this region cause a decrease in tensile-shear load – crosshead displacement values and also the brittle fracture areas in the SEM analysis of the fractured surfaces (Figure 11b). It is estimated that the D6 sample broke off from the coarse-grained region, which is thought to be composed of ferrite, tempered martensite and tempered bainite phases. Due to the increase in welding speed, the depth of penetration in this sample also decreased and at the same time, this grain coarsening was the basis of the brittle fracture morphology in the examination of the fracture surface (Figure 11c).

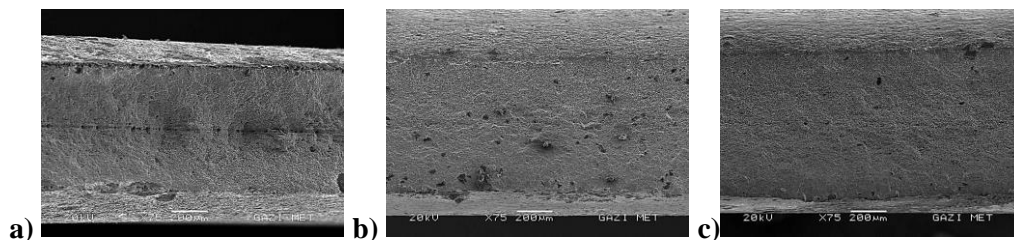


Figure 11. Fracture Surface of –1.4 mm Focal Length Specimens After Tensile - Shear Load Test, a) D4 Sample, b) D5 Sample, c) D6 Sample

4. CONCLUSION

In this study 4 kW laser power, 3, 3.5, 4 m/min welding speed and two different focal length distances (0 and –1.4 mm) parameters were used as welding parameters. Tensile-shear strength, microhardness, and fracture surfaces were examined and the influences of welding speed and focal length distances on the result of mechanical properties of the welded joints have been discussed. The following conclusions were drawn:

1. Weld joint shape is completely related to the heat input and the Lorentz forces, Marangoni and plasma shear forces. For both focal lengths, bottom penetration depths decreased when the welding speeds increased. From samples welded using different focal lengths, the FZ geometries of samples using the same welding speed are similar. Since Lorentz forces occurring due to arc pressure in the keyhole during welding are higher than Marangoni and plasma shear forces, the shrinkage cavity is at most 3.5 m/min occurred in samples with welding speed.
2. Tensile-shear strength values decreased depending on the increased welding speed for both focal length specimens. Since penetration depth and especially phase transformations has changed according to the welding speed, heating and cooling characteristics.
3. The microhardness results were affected by welding speed and focal lengths. In 0 mm focal length distance specimens' hardness values increased according to the increased welding speed and high cooling rate. But in negative focal length, cooling rate is slower than 0 mm focal length, so it is

thinking that the tempering process is occur in the bottom plate because of the lasem beam geometry and this tempering process cause tempered martensite and tempered bainite especially in the bottom plate and finally these issues cause the decreasing the hardness values when the welding speed increased.

4. All specimens were fractured from BM in 0 mm focal length and so, in SEM investigations, ductile fracture morphology and similar dimple size were observed in fracture surfaces. Since penetration depth, grain coarsening and also phase transformation, fracture zones changed according to the welding speed in negative focal length. But the specimens which are welded in -1.4 mm focal length, fracture zones got closer to the FZ when the welding speed increased.

ACKNOWLEDGEMENT

This study is supported by IPG Photonics Eurasia – Tuzla, İstanbul, Turkey.

CONFLICT OF INTEREST

The authors declares that there is no conflict of interest regarding the publication of this paper.

REFERENCES

- Aktarer, S. M., Küçükömeroğlu, T., & Davut, K. (2019). Friction stir processing of dual phase steel: Microstructural evolution and mechanical properties. *Materials Characterization*, 155, 109787. doi:[10.1016/j.matchar.2019.109787](https://doi.org/10.1016/j.matchar.2019.109787)
- ASTM International. (2010). *Standard Test Methods for Tension Testing of Metallic Materials* (ASTM E8/E8M-21) doi:[10.1520/E0008_E0008M-16A](https://doi.org/10.1520/E0008_E0008M-16A)
- ASTM International. (2012). *Standard Test Methods for Coating Mass and Chemical Analysis of Zinc-Nickel Alloy Electrolytically Coated on Steel Sheet* (ASTM E1659-12) doi:[10.1520/E1659-12](https://doi.org/10.1520/E1659-12)
- Alves, P. H. O. M., Lima, M. S. F., Raabe, D., & Sandim, H. R. Z. (2018). Laser beam welding of dual-phase DP1000 steel. *Journal of Materials Processing Technology*, 252, 498-510. doi:[10.1016/j.jmatprotec.2017.10.008](https://doi.org/10.1016/j.jmatprotec.2017.10.008)
- Çavuşoğlu, O., Toros, S., & Gürün, H. (2019). Microstructure based modelling of stress-strain relationship on dual phase steels. *Ironmaking & Steelmaking*, 46(4), 313-319. doi:[10.1080/03019233.2017.1371959](https://doi.org/10.1080/03019233.2017.1371959)
- Dai, J., Meng, Q., & Zheng, H. (2020). High-strength dual-phase steel produced through fast-heating annealing method. *Results in Materials*, 5, 100069. doi:[10.1016/j.rinma.2020.100069](https://doi.org/10.1016/j.rinma.2020.100069)
- Farabi, N., Chen, D. L., & Zhou, Y. (2011). Microstructure and mechanical properties of laser welded dissimilar DP600/DP980 dual-phase steel joints. *Journal of Alloys and Compounds*, 509(3), 982-989. doi:[10.1016/j.jallcom.2010.08.158](https://doi.org/10.1016/j.jallcom.2010.08.158)
- Ferreira, C. C. de A., Braga, V., de Siqueira, R. H. M., de Carvalho, S. M., & de Lima, M. S. F. (2020). Laser beam welding of DP980 dual phase steel at high temperatures. *Optics and Laser Technology*, 124, 105964. doi:[10.1016/j.optlastec.2019.105964](https://doi.org/10.1016/j.optlastec.2019.105964)
- Fonstein, N. (2017). 7 - Dual-phase steels. In: R. Rana & S. B. Singh (Eds.), *Automotive Steels* (pp. 169-216). Woodhead Publishing. doi:[10.1016/B978-0-08-100638-2.00007-9](https://doi.org/10.1016/B978-0-08-100638-2.00007-9)
- Gong, H., Wang, S., Knysh, P., & Korkolis, Y. P. (2016). Experimental investigation of the mechanical response of laser-welded dissimilar blanks from advanced- and ultra-high-strength steels. *Materials & Design*, 90, 1115-1123. doi:[10.1016/j.matdes.2015.11.057](https://doi.org/10.1016/j.matdes.2015.11.057)
- Hong, K., & Shin, Y. C. (2017). Prospects of laser welding technology in the automotive industry : A review. *Journal of Materials Processing Technology*, 245, 46-69. doi:[10.1016/j.jmatprotec.2017.02.008](https://doi.org/10.1016/j.jmatprotec.2017.02.008)
- ISO (2016). *Resistance welding - Destructive testing of welds - Specimen dimensions and procedure for cross tension testing of resistance spot and embossed projection welds* (ISO 14273:2016) www.iso.org/standard/61273.html

- ISO (2019). *Metallic materials - Tensile testing - Part 1: Method of test at room temperature* (ISO 6892-1:2019) www.iso.org/standard/78322.html
- Kundu, J., Ray, T., Kundu, A., & Shome, M. (2019). Effect of the laser power on the mechanical performance of the laser spot welds in dual phase steels. *Journal of Materials Processing Technology*, 267, 114-123. doi:[10.1016/j.jmatprotec.2018.12.014](https://doi.org/10.1016/j.jmatprotec.2018.12.014)
- Kuril, A. A., Jagannatham, M., Janaki Ram, G. D., & Bakshi, S. R. (2019). Effect of Post - Weld Heat Treatment on the Microstructure of Plasma Arc Welded DP600 Steel. *Metallography, Microstructure, and Analysis*, 8(6), 848-860. doi:[10.1007/s13632-019-00590-9](https://doi.org/10.1007/s13632-019-00590-9)
- Lakshminarayana, P., Gautam, J. P., Mastanaiah, P., Reddy, G. M., Rao, K. B. S. (2018). Influence of beam power and Traverse speed in Fibre Laser welding of dual Phase steel (590) on depth of WELD zone penetration, microstructure and hardness. *Materials Today: Proceedings*, 5(9), 17132-17138. doi:[10.1016/j.matpr.2018.04.121](https://doi.org/10.1016/j.matpr.2018.04.121)
- Mitra, S., Arora, K. S., Bhattacharya, B., & Singh, S. B. (2020a). Effect of Welding Speed on Texture in Laser-Welded Dual-Phase Steel. *Metallurgical and Materials Transactions A*, 51(6), 2915-2926. doi:[10.1007/s11661-020-05747-8](https://doi.org/10.1007/s11661-020-05747-8)
- Mitra, S., Arora, K. S., Bhattacharya, B., & Singh, S. B. (2020b). Effect of Welding Speed on the Prediction Accuracy of Residual Stress in Laser Welded 1.2 mm Thick Dual Phase Steel. *Lasers in Manufacturing and Materials Processing*, 7(1), 74-87. doi:[10.1007/s40516-019-00107-w](https://doi.org/10.1007/s40516-019-00107-w)
- Palanivel, R., Dinaharan, I., & Laubscher, R. F. (2020). Microstructure and mechanical behavior of Nd:YAG laser beam welded high strength low alloy steel joints. *Optik*, 208, 164050. doi:[10.1016/j.ijleo.2019.164050](https://doi.org/10.1016/j.ijleo.2019.164050)
- Sun, Q., Di, H. S., Li, J. C., & Wang, X. N. (2016). Effect of pulse frequency on microstructure and properties of welded joints for dual phase steel by pulsed laser welding. *Materials & Design*, 105, 201-211. doi:[10.1016/j.matdes.2016.05.071](https://doi.org/10.1016/j.matdes.2016.05.071)
- Švec, P., Schrek, A., Hrnčiar, V., & Csicsó, T. (2015). Fibre Laser Welding of Dual Phase Steels. *Acta Metallurgica Slovaca*, 21(4), 311-320. doi:[10.12776/ams.v21i4.626](https://doi.org/10.12776/ams.v21i4.626)
- Tuncel, O., & Aydın, H. (2020). A Comparison of Tensile Properties of Single-Sided and Double-Sided Laser Welded DP600 Steel Sheets. *Materials Science*, 26(2), 173-178. doi:[10.5755/j01.ms.26.2.21374](https://doi.org/10.5755/j01.ms.26.2.21374)
- Kancharla, V., Mendes, M., Grupp, M., & Baird B. (2018, May 1). Recent advances in fiber laser welding. *Industrial Laser Solutions*. www.industrial-lasers.com/welding/article/16485184/recent-advances-in-fiber-laser-welding
- Wang, J., Yang, L., Sun, M., Liu, T., & Li, H. (2016). Effect of energy input on the microstructure and properties of butt joints in DP1000 steel laser welding. *Materials & Design*, 90, 642-649. doi:[10.1016/j.matdes.2015.11.006](https://doi.org/10.1016/j.matdes.2015.11.006)
- Wang, X., Sun, Q., Zheng, Z., & Di, H. (2017). Microstructure and fracture behavior of laser welded joints of DP steels with different heat inputs. *Materials Science & Engineering A*, 699, 18-25. doi:[10.1016/j.msea.2017.05.078](https://doi.org/10.1016/j.msea.2017.05.078)
- Xie, C., Yang, S., Liu, H., Zhang, Q., Cao, Y., & Wang, Y. (2017). Microstructure and Fatigue Properties of Laser Welded DP590 Dual-Phase Steel Joints. *Journal of Materials Engineering and Performance*, 26(8), 3794-3801. doi:[10.1007/s11665-017-2848-7](https://doi.org/10.1007/s11665-017-2848-7)
- Zhao, D., Wang, Y., Zhang, P., & Liang, D. (2019). Modeling and Experimental Research on Resistance Spot Welded Joints for Dual-Phase Steel. *Materials*, 12(7), 1108. doi:[10.3390/ma12071108](https://doi.org/10.3390/ma12071108)
- Zhao, Y. Y., Zhang, Y. S., Hu, W. (2013). Effect of welding speed on microstructure, hardness and tensile properties in laser welding of advanced high strength steel. *Science and Technology of Welding and Joining*, 18(7), 581-590. doi:[10.1179/1362171813Y.0000000140](https://doi.org/10.1179/1362171813Y.0000000140)